Development and analysis of non-linearity in the pressure waves resulting from thermoacoustic heat engines

Abdelmaged Ibrahim, Ahmed Elbeltagy, Mahmoud Emam, Ehab Abdel-Rahman

ACOUSTICS 2012

Development and analysis of non-linearity in the pressure waves resulting from thermoacoustic heat engines

A. H. Ibrahim[a], A. A. Elbeltagy[a], M. M. Emam[a] and E. Abdel-Rahman[a,b]

[a]The American University in Cairo, School of Sciences & Engineering, (On leave from Cairo University), 11835 New Cairo, Egypt
[b]Mechanical Power Engineering Department, Cairo University, 12613 Cairo, Egypt
abdelmaged@aucegypt.edu

Thermoacoustic heat engines are intrinsically simple, reliable, environmentally friendly and reasonably efficient. In this work, a thermoacoustic prototype was designed, built and operated and its performance indices quantified. The second law of thermodynamics dictates that higher conversion efficiencies necessitate high temperatures at the hot side of the engine's stack. This work investigates one of the limits associated with the hot side temperature, which is the excitation of higher harmonics and corresponding limitations on the dynamic pressure amplitude and conversion efficiency. It is observed that operating the engine at a temperature just above the onset temperature generates an acoustic wave at the fundamental mode with no harmonics observed but with relatively low dynamic pressure amplitude. As the hot-side temperature increases, higher harmonics are excited causing distortions in the resulting acoustic wave. The excitation of the harmonics at increasing temperatures is quantified and analyzed. For example, as the temperature difference across the stack increases by 140 % from 235 ^{o}C to 567 ^{o}C, the ratio of the pressure amplitude of the first harmonic to that of the fundamental mode increases by 950 %, from 0.04 to 0.38. At the temperature difference of 567 ^{o}C across the stack, approximately 30 % of the generated acoustic power is contained in the first mode. Furthermore, analysis of the measured AC-coupled dynamic pressure waves shows that the distorted waves can be numerically re-constructed by considering only the fundamental mode and the first three harmonics, indicating that at the operation range considered the harmonics were the main source of non-linearity.

1 Introduction

A thermoacoustic engine uses the interaction of thermodynamics and acoustics to convert heat supplied at a temperature gradient across a porous medium into a high-amplitude pressure wave, which is one form of mechanical work. It consists basically of a porous medium (known as a stack) carefully positioned between two heat exchangers and this whole assembly placed inside a resonator that contains the resulting acoustic wave.

The conversion of heat into a pressure wave in standing-wave thermoacoustic engines relies on the ability of the compressible working gas in the engine to follow a Brayton's thermodynamic cycle in the vicinity of the stack wall due to the properly-phased pressure and velocity oscillations. Such an engine converts heat power into acoustic power without the need of a piston-cylinder arrangement, sliding seal or harmful working fluids and therefore it enjoys high reliability, low maintenance and low cost. The advantages of these engines have led to a considerable research to increase the efficiency and power density of these engines.

Figure 1 shows a schematic of a half-wave length standing wave engine. The figure shows the stack positioned between a hot heat exchanger (which supplies the heat to the stack) and an ambient heat exchanger (which rejects the waste heat to the ambient). For the pressure wave to be generated, the temperature gradient per unit length of the stack must exceed a certain critical temperature gradient, given by [1]

$$\nabla T_{cri} = \frac{p_1 \omega}{\rho \, c_p u_1} \qquad (1)$$

Where p_1 is the dynamic pressure, u_1 is the local oscillating velocity of the acoustic wave, ρ is the mean density of the gas, c is the specific heat, and ω is the angular frequency of the wave ($\omega=2\pi f$).

The critical temperature of the hot-side of the stack, below which the wave is not generated, is known as the onset temperature. The critical temperature difference across the stack below which the wave is not generated is referred to as the critical temperature difference.

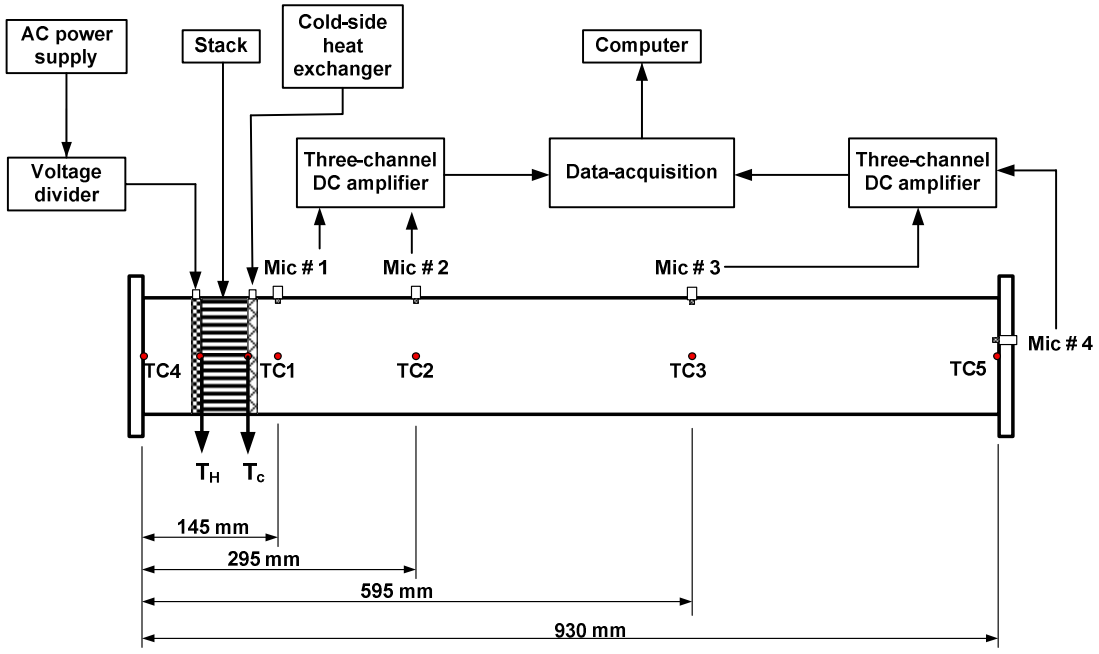

Figure 1: A schematic of the thermoacoustic engine and its measuring instruments

The design and manufacturing of the two heat exchangers surrounding the stack are critical to sustain the wave generation because they maintain the temperature difference across the stack through proper supply of heat at one side and enough rejection of heat at the other side. Thedesign and manufacturing of heat exchangers for thermoacoustic devices are explained in details in [2]

For standing-wave thermoacoustic engine, a first-law efficiency of 18% was reported by Godshalk *et al.* [3] and a second-law efficiency of 30% was reported by Gardner and Swift [4].

Commercial products employing thermoacoustics currently are being generated. For example, Score Ltd. was awarded £2M in 2007 to research a cooking stove that delivers electricity and cooling using the thermo-acoustic effect for use in developing countries [5]. Typical applications of thermoacoustic engines require that the resultant pressure wave is generated and sustained at a controlled frequency so that the dominant part of the acoustic power in the wave is at the fundamental frequency, with very minor to no contribution of higher harmonics. For example, if the engine is to drive a thermoacoustic refrigerator or a heat pump, it must provide a pressure wave at the resonance frequency required by the driven device. Small deviations may be tolerated, depending on the Q-factor of the thermoacoustic refrigerator/heat pump [6]. A similar requirement is needed if the engine is to drive a linear alternator to generate electricity. Therefore, excitation of the harmonics is generally undesirable and should be suppressed.

The second law of thermodynamics dictates that high operating temperatures tend to increase the conversion efficiency. The thermoacoustic engines enjoy a main advantage, which is the lack of moving parts, allowing higher operating temperatures. However, other limits such as the fact that only the acoustic energy in the fundamental mode is useful should be considered. Therefore, there is a need to quantify the generation of higher harmonics as the hot-end temperature increases, because the acoustic energy associated with the harmonics will not be of use and should be eliminated or suppressed.

The harmonics are generated because of the non-linear terms in the Navier-Stokes equations, such as the product of the dynamic density and the gas parcel velocity, which are both first-order terms. Each of these terms has a cos (ωt) dependence, and their product causes a cos (2ωt) dependence because cos (ωt) X cos (ωt) = 0.5 [1+ cos (2ωt)]. Once the (2ωt) waves exist, they interact with the fundamental mode oscillating at the angular frequency ω, giving rise to 3ω oscillations because cos (ωt) X cos (2ωt) = 0.5 [cos (ωt) + cos (3ωt)].

Now, for an iso-diameter resonator, where the cross-sectional area is independent of the axial location along the entire length, the harmonics are multiple integers of each others. The excitation of the harmonics can be suppressed via the use of tapered or anharmonic resonators [7-8]. Variable-diameter resonators provide another advantage by reducing the viscous losses. The present work utilizes an iso-diameter resonator to provide a base case for which the suppression of harmonics via different resonator shapes can be compared.

The objective of this work is to quantify the excitation of the harmonics as the operating temperature increases in an iso-diameter resonator, such that that more complicated resonator shapes can be evaluated against it. The excitation of harmonics is evaluated through the wave decomposition into a fundamental mode and higher harmonics, through fast Fourier transformations and through evaluation of acoustic powers available in each mode.

A schematic of the experimental setup isshown in figure 1.The stack is 4 cm long, has 600 cells per square inch, a wall thickness of 76.2μm, is made of celor and is supplied by Corning. The stack is positioned between two home-made heat exchangers. One side of the stack is heated using an electric heater connected to a voltage divider (2 kVA Power rating) to allow control of the input electric power fed to the engine and corresponding control of the hot-side temperature of the stack. To maintain the temperature gradient across the stack, the other side of the stack is cooled via a home-made heat exchanger made of six-path 6-mm inside diameter copper tubes with six copper fins at one side and an aluminum mesh on the other side. The water flow rate through this heat exchanger at the operating conditions used in this work is 0.16 kg/s.

The trade-offs between dynamic pressure distribution, gas parcel velocity distribution, viscous losses and thermal relaxation losses typically position the stack and the two heat exchangers in the first quarter of the resonator. In thiswork, the stack is placed 50 mm away from the left blind flange shown in figure 1. The stack and the two heat exchangers are housed inside a 930-mm long resonator of an *iso-diameter* of 128 mm.

The temperatures at the hot and cold sides of the stack are measured with thermocouples (type K, 147 μm in diameter, supplied by Omega Engineering). The dynamic pressures at different axial locations 14.5 cm, 30.5 cm, 59.5 cm and 93 cm) inside the engine are measured using pressure microphones. The axial locations where the microphones are positioned correspond to 0.78 %, 1.64 % and 3.2 %, respectivley of the wave length. The presure microphones used are piezo-resistive Meggitt microphones (Model 8510B-2, range 0-2 psi gage, individually calibrated, sensitivity of about 20 mV/kPa, resonance frequency of 70 kHz and high stability over temperature transients).

The signals from the pressure transducer are fed into a three-channel, 200 kHz bandwidth, programmable-gain DC amplifier.

Both temperature and pressure signals are acquired simultaneously using a USB data acquisition board (Omega model OMB-DAQ-3005, 16-bit, 16differential channels, 1-MHz band width, with programmable gain). These measurements allow capturing of the hot and cold stack temperatures as well as the resultant dynamic pressure amplitude at different axial locations. More details of the experimental setup can be found in related experimental work by the authors [9-11]. Numerical work by the authors on thermoacoustic engines can be found in [12-14].

The measured data allows estimation of the onset temperature and the acoustic power via the two-microphone method [15]. It also makes it possible to decompose the AC-coupled pressure wave into a fundamental mode and higher harmonics, according to the form

$$P(t) = P_0 \sin(2\pi f_0 t + \varphi_0) + P_1 \sin(2\pi f_1 t + \varphi_1) + P_2 \sin(2\pi f_2 t + \varphi_2) + P_3 \sin(2\pi f_3 t + \varphi_3) \quad (2)$$

The determination of the pressure magnitude and phase of each mode at each microphone location allows estimation of the average acoustic power between any two microphones [15]for the fundamental mode and the first harmonic.

The two microphone method is limited by the fact that phase mismatch between the two measuring microphones can introduce significant error. Reference [15] suggested that the microphones should be placed such that there is at least one degree in phase difference between the two pressure signals.

2 Results

First, it is beneficial to carefuly observe the measured AC-coupled pressure waves in the time-domain. Figure 2 shows the resulting dynamic AC-coupled pressure waves in a range of hot-end temperature from 340 ^{o}C to 648 ^{o}C for the first, second and third microphones. Looking at the pressure data presented in case (A), where the engine is operating at a temperature difference of 235 ^{o}C, just six percents above its onset temperature difference of 221^{o}C, it is observed that the wave measured with the first microphone, the nearest to the pressure antinode, indicates a pure sine wave with an amplitude of 328 Pa and a frequency of 190.4 Hz. At the same operating conditions but further along the axis of the resonator, the amplitude reduces and the wave is more and more distorted. For example, the third microphone located the farthest from the pressure antinode reads an amplitude of 150.6 Pa and its harmonic analysis show two frequencies, namely190.4 Hz and 380.9 Hz.

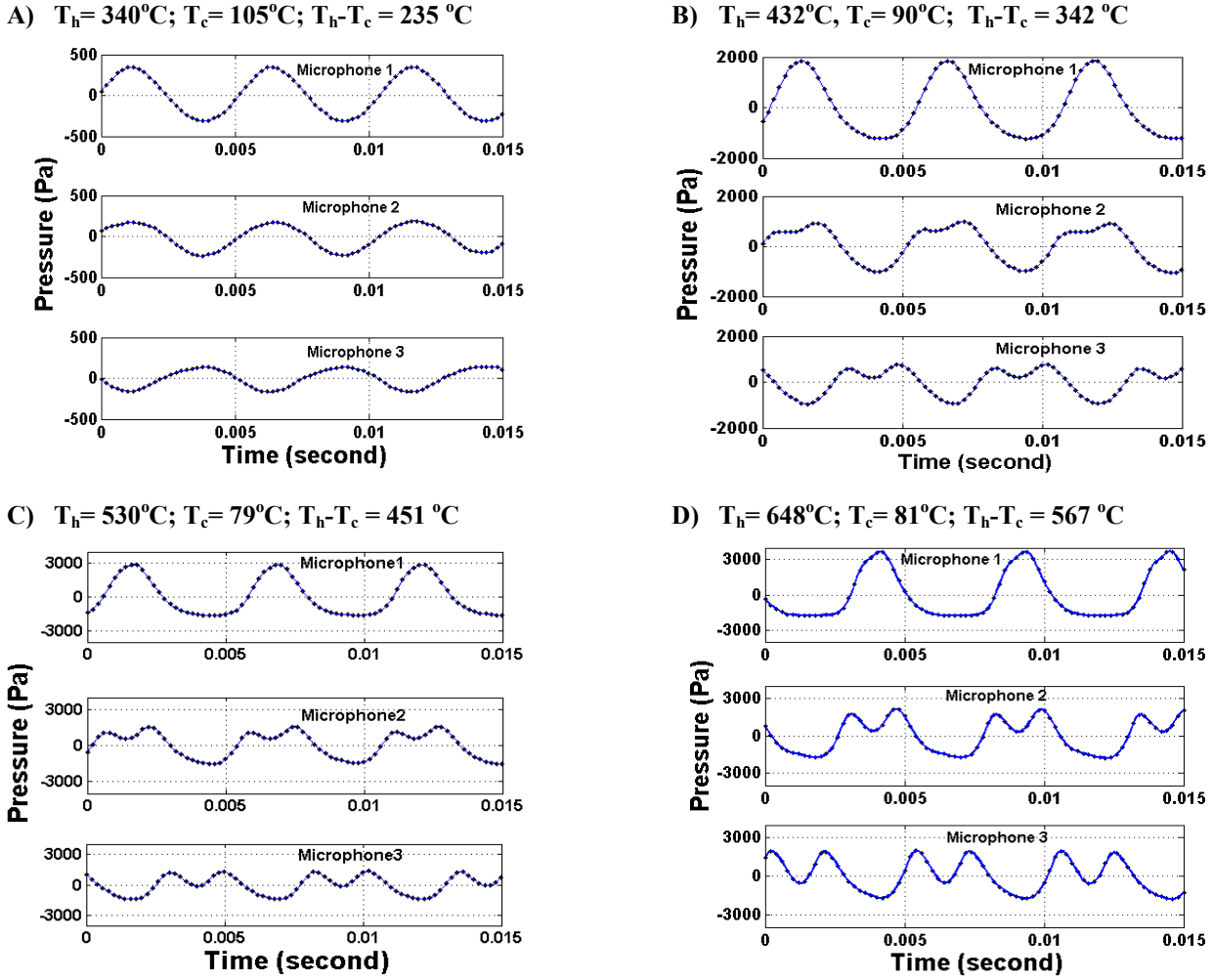

Figure 2: AC-coupled pressure waves in the time domain at different temperature differences across the stack at three different axial locations along the resonator

The reduction of pressure amplitude along the resonator axis is because of the nature of pressure distribution along the resonaotor axis for different modes. The increase in the harmonic content in the third microphone with respect to the first microphine is because the first harmonic has its pressure antinode at the resonator middle, as opposed to the fundamental mode which has its pressure antinodes at the resonator ends, as shown in figure 3. Therefore, around the middle of the resopnator the first harmonic dominates over the fundamental mode which explains the increase in the wave distortation as the pressure measurements approach the middle of the resonator.

As the hot-end temperature increases, the pressure wave measured by the first microphone experiences more distortions, indicating higher excitation of the harmonics. The pressure wave captured by the second and third microphones always shows more distortion than that measured by the first microphone, as explained above. In this work, the captured pressure wave is decomposed into a fundamental mode and higher harmonics, as illustrated by

equation (1). This decomposition is performed using non-linear best fitting to reduce the sum of squared-deviations between the measured signal and the form illustrated in equation (1). This form fits the signal reasonably with a typical R^2 value of 0.99 or higher. A visual inspection of the accuracy of the fit can be viewed in figure 2 where the symbols show the measured data points and the solid curve shows the fit. Some results are shown in table 1.

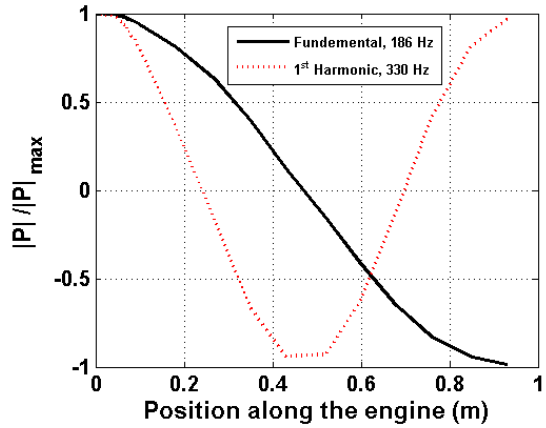

Figure 3:Theoretical distribution of the pressure magnitudes of the fundamental mode and the first harmonic velocity magnitudes of the fundamental mode.

The decomposition of the wave into a fundamental mode and higher harmonics provides information on the pressure magnitude and phase of each mode. This also allows estimation of the acoustic power contained in each mode.

Comparison between cases (A) and (D) in figure 2 shows that as the temperature difference across the stack increases from 235°C to 567°C, the pressure magnitude of the fundamental component P_0 increases from 301 Pa to 2577 Pa, while the pressure magnitude P_1 of the first harmonic component increases from 13 Pa to 972 Pa. The P_1/P_0 ratio indicates the relative strength of the first harmonic to the fundamental mode increases by an order of magnitude, from 0.04 to 0.38. Similarly, the ratio of the pressure magnitude of the third harmonic to that of the fundamental (P_3/P_0) increases by more than an order of magnitude from 0.2% to 3%. This illustrates how the increase in the operating temperature causes an increase in the dynamic pressure of the resulting pressure wave but also causes increased excitation of the harmonics.

Table 1: Regression results for the waves in figure 2

	T_h-T_c = 235 °C	T_h-T_c = 342 °C	T_h-T_c = 451 °C	T_h-T_c = 567 °C
f	190.4	191.3	191.4	192.7
P_0	301.6	1554	2204	2577
P_1	13	317	652	972
P_2	0.3	23	74	157
P_3	0.6	11	42	86
P_1/P_0	0.04	0.20	0.30	0.38
φ_0	-21.6	8.7	17.0	21.2
φ_1	-107	-55.2	-44.1	-39.5
φ_2	-216	-96.4	-81.5	-79.5
φ_3	0.0	2.8	30.7	40.6

A) T_h= 340°C; T_c= 105°C; T_h-T_c = 235 °C

B) T_h= 432°C, T_c= 90°C; T_h-T_c = 342 °C

C) T_h= 530°C; T_c= 79°C; T_h-T_c = 451 °C

D) T_h= 648°C; T_c= 81°C; T_h-T_c = 567 °C

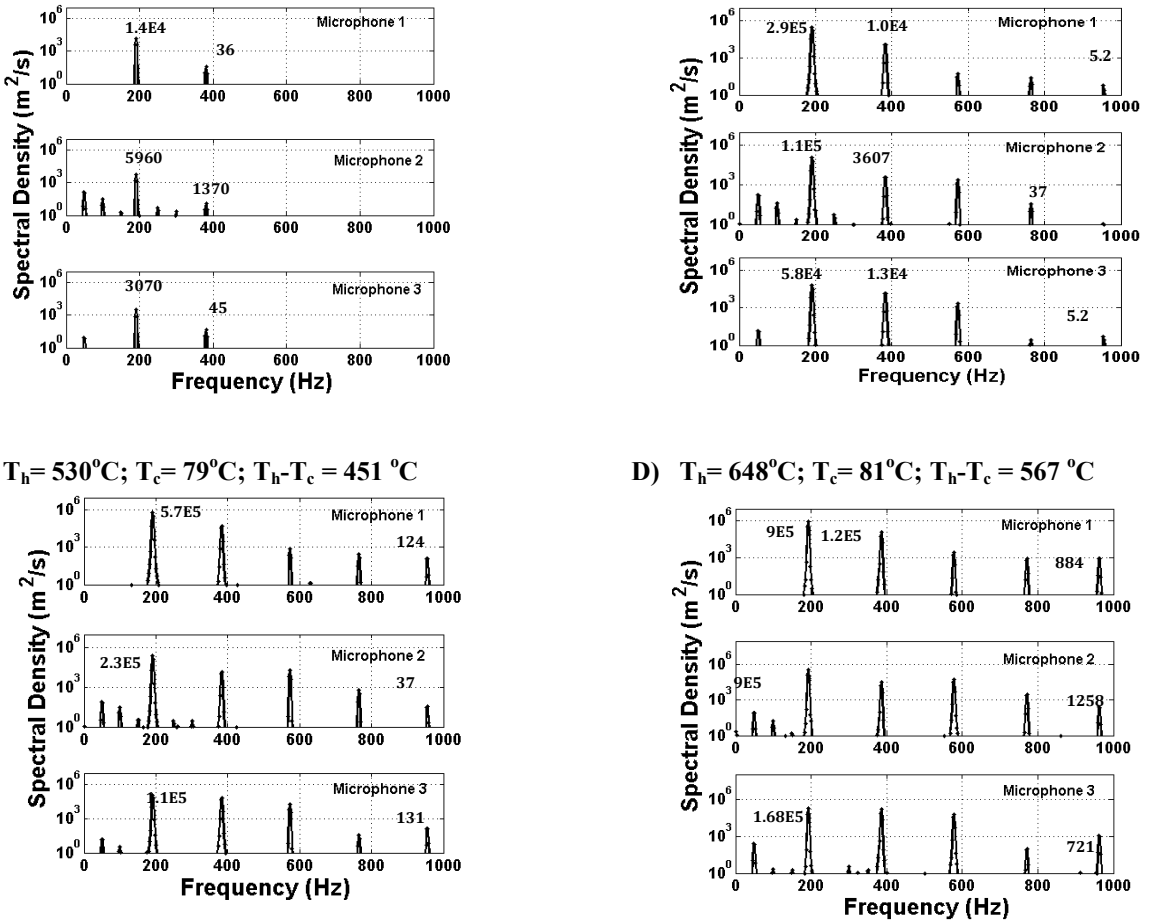

Figure 4: The data of figure 2 plotted in frequency domain

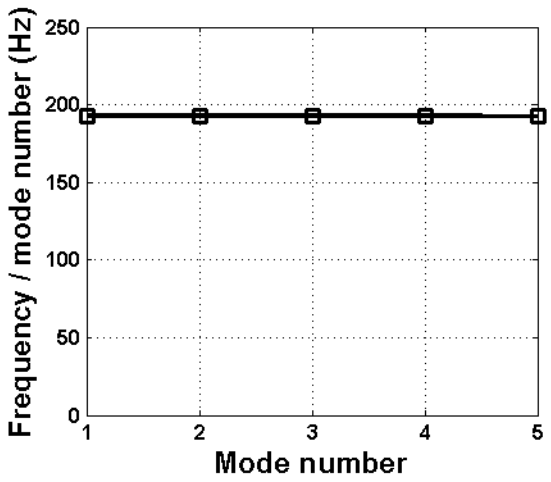

Figure 5: The frequency divided by the mode number of the fundametal wave and the harmonics

The data presented in the time domain in figure 2 is further analysed in the frequency domain and the results plotted in figure 4. In this analysis, a set of 2048 data points are used for each case with a sampling rate of 5 kS/s, yielding a frequency resolution of 2.4 Hz. In figure 4, a vertical logarithmic scale is used extending from 1 to 2E6 to showing the large range of the spectral density of the components of the pressure wave, particularly at high temperatures. The results show the frequency of the fundamental mode (190.4 Hz) and the frequency of the higher harmonics (382.6 Hz, 574.2 Hz and 770.8 Hz). The progression of the harmonics with the increase of hot-end temperature is demonstrated.

For example, the ratio of the spectral density of the first harmonic to that of the fundamental increases from 36/1.4E4 = 2.57E-3 in case A, where the hot-end temperature is 340 ^{o}C. In case D, where the hot-end temperature is 648 ^{o}C, this ratio becomes 1.2E5/9E5 = 0.13.

Further analysis is made on the frequency content of the harmonics in the iso-diameter resonator used in this work. Figure 5 shows the frequency of each mode divided by the mode number on the vertical axis and the mode number on the horizontal axis. This plot indicates that the harmonics are multiple integers of each others, to within the frequency resolution of 2.4 Hz, which is a consequence of the use of an iso-diameter resonator.

Because the numerical decomposition of the captured pressure wave allows estimation of the pressure magnitude of each mode, it is possible to investigate the progression of the pressure magnitudes versus the temperature difference. Figure 6 shows this progression at each of the three microphone locations.

The ratio of the dynamic pressure amplitudes of the first harmonic to that of the fundamental mode increases almost linearly with the temperature difference across the stack, as shown in figure 7.

The increase in the total acoustic power with the temperature difference cross the stack is evident in figure 8, but the ratio of the power contained in the first harmonic to the total becomes more significant as the operating temperature increases.

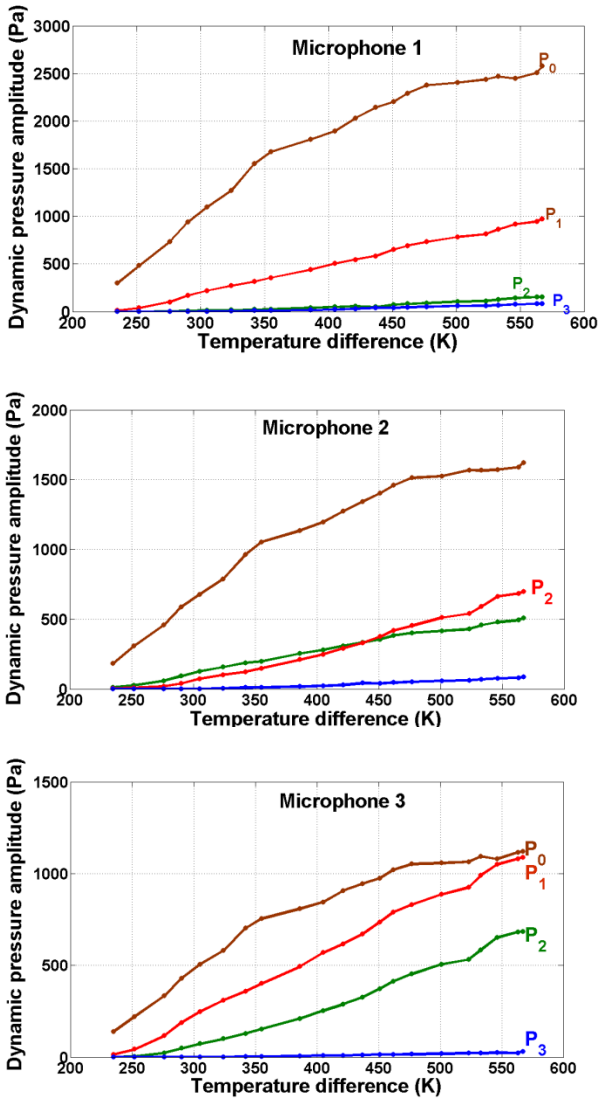

Figure 6: Variation of pressures of the fundamental and higher harmonics versus the temperature difference across the stack for each of the three microphones

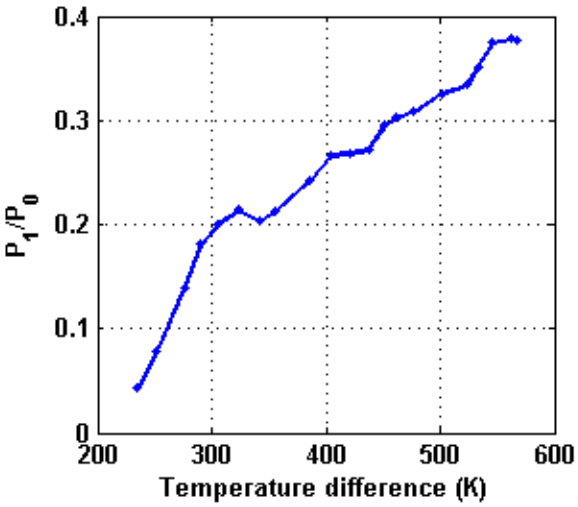

Figure 7: Development of the ratio of the dynamic pressure amplitudes of the first harmonic to the fundamental mode versus the temperature difference across the stack

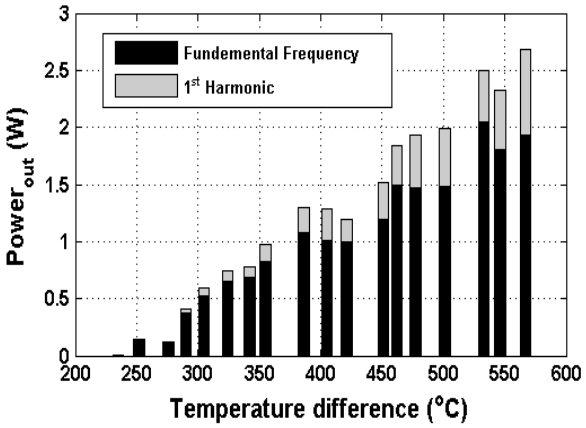

Figure 8: Development of the acoustic power in the fundamental mode and the first harmonic versus the temperature difference across the stack

3 Summary and Conclusion

This work presents experimental results on the excitation of higher harmonics with the engine operating temperature. The acquired pressure wave is decomposed into a fundamental mode and three harmonics. The development of the dynamic pressure amplitude with the increase in the temperature difference across the stack is presented. The results show that the AC-coupled pressure wave can be reconstructed numerically by considering only the fundamental mode and the first three harmonics, indicating that the harmonics are the main source of non linearity at these operating conditions. Furthermore, the loss in the dynamic pressure amplitude and acoustic power generated due to the harmonic excitations is quantified. For example, as the temperature difference across the stack increases by 140% from 235 ^{o}C to 567 ^{o}C, the ratio of the pressure amplitude of the first harmonic to that of the fundamental mode increases by 950%, from 0.04 to 0.38. At the temperature difference of 567 ^{o}C across the stack, approximately 30 % of the generated acoustic power is contained in the first mode. The analysis in the frequency domain indicates that the harmonics are multiple integers of each others, which is expected in this iso-diameter resonator shape. The provided data presents a base case against which different resonator shapes can be evaluated in terms of their ability to suppress harmonic excitation.

References

[1] G. W. Swift. Thermoacoustic engines. *J Acoustics Soc Am.* Vol. 84, pp. 1146–80, 1988.

[2] S. L. Garrett, D. K. Perkins, and A. Gopinath, ‘‘Thermoacoustic refrigerator heat exchangers: design, analysis and fabrication. *Proceedings 10th International Heat Transfer Conference*. Vol. 4, pp. 375–380, 1994

[3] K. M. Godshalk, C. Jin, Y. K. Kwong, E. L. Hershberg, G. W. Swift, R. Radebaugh, “Characterization of 350 Hz thermoacoustic driven orificepulse tube refrigerator with measurements of the phase of the mass flow and pressure,” *Adv. Cryo. Eng*., vol. 41, pp. 1411-1418, 1996.

[4] D.L. Gardner, G.W. Swift, “A Cascade thermoacoustic engine” *J. Acoust. Soc. Am.,* vol. 114, no. 4, pp. 1905 -1919, 2003.

[5] SCORE (Stove for Cooking, Refrigeration and Electricity), http://www.score.uk.com/research/default.aspx, last checked in March 2012.

[6] T. Biwa, Y. Ueda, H. Nomura, U. Mizutani, T. Yazaki, “Measurement of the Q value of an acoustic resonator”, *Physical Review E*, vol. 72, pp. 026601 - 026606, 2005.

[7] E.C.Luo, H.Ling, W.Dai, G.Y.Yu, “Experimental study of the influence of different resonators on thermoacoustic conversion performance of a thermoacoustic-Stirling heat engine”, *Ultrasonics*, vol. 44, e1507 - e1509, 2006.

[8] M. A. Nouh, N. M. Arafa, K. Larsson, E. Abdel-Rahman. “Design study of anharmonic standing wave thermoacoustic heat engine”, *The Sixteenth International Conf. on Sound and Vibration*. 5 - 9 July 2009. KraKow, Poland.

[9] A. H. Ibrahim, E. Abdel-Rahman, “Innovative solar-energy-driven power converter: efficient operation of thermoacoustic engines”, The 2nd International Conference on Renewable Energy: Generation and Applications, AlAin, UAE, 4 - 7 March, 2012.

[10] A. H. Ibrahim, M. Emam, A. Elbeltagy, H. Omar, E. Abdel-Rahman, “Performance evaluation of thermoacoustic engine using different gases”, *9th International Congress on Sound and Vibration (ICSV19)*, accepted for publication, Vilnius, Lithuania, 8 – 12 July, 2012.

[11] A. H. Ibrahim, M. Emam, A. Elbeltagy, E. Abdel-Rahman, “Transient response and hysteresis thermo-acoustic engines”, *Sixth Heat Powered Cycles Conf., accepted for publication*, ECN, Netherlands, 10 – 12 Sept., 2012.

[12] N. M. Arafa, A. H. Ibrahim, E.E. Khalil, “Sensitivity analysis of a standing-wave thermoacoustic engine”, *9th Annual International Energy Conversion Engineering Conference.* 31 July - 03 August 2011, San Diego, California. AIAA 2011- 5802.

[13] N. M. Arafa, A. H. Ibrahim, K.Addas, Ehab Abdel-Rahman, “Design considerations for thermoacoustic engines for low onset temperature and efficient operation”, *Forum Acusticum*. 27 June - 1 July, 2011, Aalborg, Denmark.

[14] A. H. Ibrahim, N.M. Arafa and E. E. Khalil Geometrical Optimization of Thermoacoustic Heat Engines. *49th AIAA Aerospace Sciences Meeting*. AIAA 2011-129. 4-7 January 2011 Orlando, Florida.

[15] T. Biwa, Y. Tashiro, H. Nomura, Y. Ueda, T. Yazaki, “Experimental verification of a two-sensor acoustic intensity measurement in lossy ducts”, *J. Acoust. Soc. Am.*, Vol. 124, No. 3, 2008.